Investigation of Protein Detection Parameters Using Nanofunctionalized Organic Field-Effect Transistors

Mallory L. Hammock,[†] Oren Knopfmacher,[†] Benjamin D. Naab,[‡] Jeffrey B.-H. Tok,[†] and Zhenan Bao[†,*]

[†]Department of Chemical Engineering and [‡]Department of Chemistry, Stanford University, Stanford, California 94305, United States

ABSTRACT Biodetection using organic field-effect transistors (OFETs) is gaining increasing interest for applications as diverse as food security, environmental monitoring, and medical diagnostics. However, there still lacks a comprehensive, empirical study on the fundamental limits of OFET sensors. In this paper, we present a thorough study of the various parameters affecting biosensing using an OFET decorated with gold nanoparticle (AuNP) binding sites. These parameters include the spacing between receptors, pH of the buffer, and ionic strength of the buffer. To this end, we employed the thrombin protein and its corresponding DNA binding aptamer to form our model detection system. We demonstrate a detection limit of 100 pM for this protein with high selectivity over other proteases *in situ*. We describe herein a feasible approach for protein detection with OFETs and a thorough investigation of parameters governing biodetection events using OFETs. Our obtained results should provide important guidelines to tailor the sensor's dynamic range to suit other desired OFET-based biodetection applications.

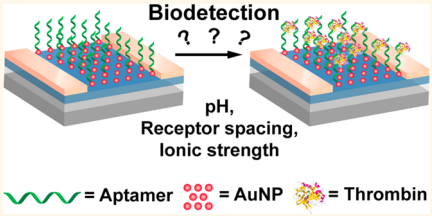

KEYWORDS: organic field-effect transistors · biodetection · screening length · nanoparticles · receptor density

Affordable healthcare is becoming a global concern of unprecedented proportions, and as a result, the need for real-time, label-free, cheap, and portable biosensors continues to increase.[1] Owing to their low cost and high efficiency, biosensors that can directly transduce a biological binding event or biological reaction into an electronic signal in a label-free manner are advantageous for sensor technologies demanding digital readout.[2,3] Miniaturizability, low-power requirements, and lack of dependence on bulky supporting electronics make electrical transducers such as electrodes, chemiresistors, and FETs promising for point-of-care diagnostics.[2,4−6] Of these transducers, FETs alone offer the additional advantages of multiparameter readout (source-drain current (I_{DS}), charge carrier mobility (μ), *etc.*) and signal amplification[7−9] and have already demonstrated much promise as (bio)chemical sensors.[2,7−15] While OFETs have historically been used for detection in the gas phase, water stability is an important consideration for biodetection that has only recently been addressed. A series of key advancements such as intrinsically water-stable semiconductors and ultrathin polymer dielectrics have allowed for the development of water-stable OFETs[10−12] that operate without the need for electrode encapsulation.[16] Finally, OFETs offer the advantages of compatibility with flexible substrates and solution processing techniques, qualities that make them suitable for low-cost, point-of-care detection and quick screening applications.

We have recently developed an OFET sensor platform that is capable of stable operation in an aqueous environment.[12] Decoration of this OFET with an ordered array of AuNPs, cast from a self-assembled poly(styrene-*b*-2-vinylpyridine) (PS-P2VP) matrix, allows for selective detection of targeted analytes.[17] Using the above-described AuNP-decorated OFET platform, we previously explored the detection of a chemical species (Hg^{2+}) in deionized water. However, the transition from chemical to biological detection remains a challenging task; in particular, protein detection using OFETs largely remains an unexplored area. To the best of our knowledge, only a single report in literature has addressed this important issue.[10] In this previous work, an antibody was detected *via* its interaction with a protein that had been immobilized on the surface of a perfluorinate-passivated pentacene transistor. The main advantage of the system used in this current study is that the organic semiconductor

* Address correspondence to zbao@stanford.edu.

Received for review December 20, 2012 and accepted April 18, 2013.

Published online April 18, 2013
10.1021/nn305903q

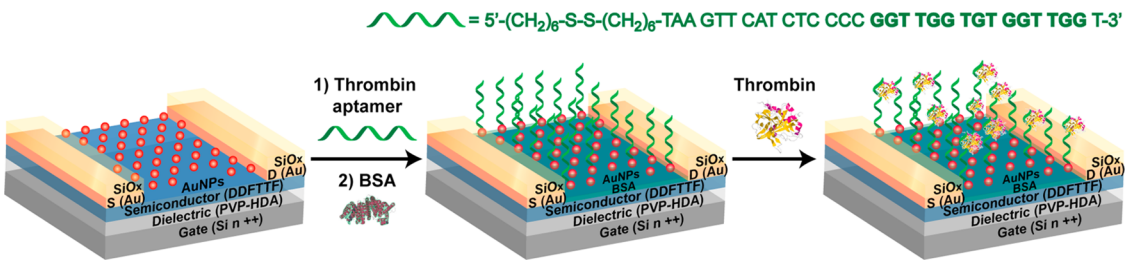

Scheme 1. Functionalization of OFET sensing platform and selective detection of target protein. A water-stable OFET is fabricated with an ultrathin PVP-HDA dielectric and DDFTTF active layer, and the electrodes are protected with a thin layer of SiO_x. The OFET is decorated with an ordered array of AuNPs to provide functionalization sites. A thrombin-specific aptamer is attached to the AuNPs *via* a Au−S linkage, and the device surface is blocked against nonspecific protein adsorption with BSA. Upon exposure to the target protein, the aptamers bind thrombin. Basepairs in bold are responsible for imparting selectivity for thrombin.

is inherently air- and water-stable, so that it does not require a passivation layer, allowing for more intimate contact between the analyte and semiconductor. One other group has used a protein-functionalized interlayer in their OFET but has only reported the detection of small molecules in the dry state with this platform thus far.[13]

Biodetection is inherently difficult due to its necessity to operate in buffer solutions and the susceptibility of biomolecules to denature or degrade over extended periods of time. In this work, we demonstrate *in situ* thrombin detection with DNA aptamers using an OFET. In addition, we present the results of a comprehensive investigation of the key parameters affecting protein detection with OFETs using thrombin as a model system. These parameters include (1) ionic strength of the buffer solution,[18−22] (2) average center-to-center distance between the receptor sites (d_{avg}), and (3) pH of the buffer solution.[10,23−26] The influence of ionic strength has been individually studied with previously reported organic electrochemical transistors (OECTs),[27] dual-gate OFETs,[28] and electrolyte-gated OFETs (EGOFETs).[29−32] Here, we report the comprehensive effect of pH, receptor spacing, and ionic strength on biodetection. Unlike inorganic FETs, investigators have yet to find any experimental studies using OFETs that carefully probe all of the above variables. Moreover, studies thoroughly investigating multiple factors using inorganic FETs have only been done *in silico*.[33,34] Here, we systematically and empirically investigate how each of these factors affects the detection of our model thrombin/DNA aptamer binding system to allow researchers to better understand and approach other OFET-based biodetection events.

RESULTS AND DISCUSSION

Sensor Fabrication and Functionalization. Devices were fabricated as previously described,[12,17] with an ultrathin dielectric layer, poly(4-vinylphenol) (PVP) cross-linked with 4,4′-(hexafluoroisopropylidene)dipthalic anhydride (HDA), and a water-stable organic semiconductor, 5,5′-bis-(7-dodecyl-9*H*-fluoren-2-yl)-2,2′-bithiophene (DDFTTF), which permits the device's operation underwater (Scheme 1). The source (S) and drain (D) electrodes were protected with a 50 nm layer of SiO_x in order to reduce parasitic currents as well as DNA binding at the electrodes. The surface of the platform was decorated with an ordered array of AuNPs cast from a PS-P2VP matrix, as previously described.[17]

A unique feature of the AuNP templating technique is that d_{avg} can be easily tuned by varying the molecular weight (M_n) of the PS-P2VP matrix from which they are cast. In this work, three M_n of PS-P2VP were used, namely, 34 kDa (M_n(PS) = 23.6 kDa, M_n(P2VP) = 10.4 kDa), 105 kDa (M_n(PS) = 55 kDa, M_n(P2VP) = 50 kDa), and 1376 kDa (M_n(PS) = 1300 kDa, M_n(P2VP) = 76 kDa). By characterization with scanning electron microscopy (SEM), the average nanoparticle diameter (D_{AuNP}) was determined to be 4.8 ± 0.6, 10.3 ± 0.9, and 10.1 ± 3.6 nm for AuNPs cast from 34, 105, and 1376 kDa PS-P2VP, respectively (Supporting Information, Figure S1 and Table S1). As determined by atomic force microscopy (AFM), d_{avg} was measured to be 39.4 ± 0.2, 70.4 ± 0.6, and 158.7 ± 8.0 nm for AuNPs cast from the 34, 105, and 1376 kDa PS-P2VP, respectively (Supporting Information, Table S2). For simplicity, we refer to these values as d_{avg} ∼40, ∼70, and ∼160 nm, respectively.

Functionalization of the AuNPs with a thiolated DNA aptamer that had previously demonstrated high affinity for thrombin[35−37] was performed in accordance with literature procedures.[17] Spectrophotometric quantification of the DNA released from the AuNPs after treatment with 100 mM NaCN was used to determine the DNA loading on the AuNPs, which was calculated to be 2.9 ± 0.5 DNA strands/AuNP and 9.2 ± 1.8 DNA strands/AuNP for AuNPs cast from the 34 and 105 kDa PS-P2VP, respectively (Supporting Information, Table S3 and Figure S2). It was not possible to quantify the DNA loading on the AuNP cast from 1376 kDa PS-P2VP due to its dilute concentration on the surface; however, it is likely similar to that reported for the AuNPs cast from the 34 and 105 kDa PS-P2VP based on their comparable diameters. The surface of the OFET was then blocked with bovine serum albumin (BSA) in order to prevent nonspecific protein adsorption (Supporting Information, Figure S3).[38]

Successful functionalization of the AuNPs with the thrombin aptamer and subsequent deposition of BSA

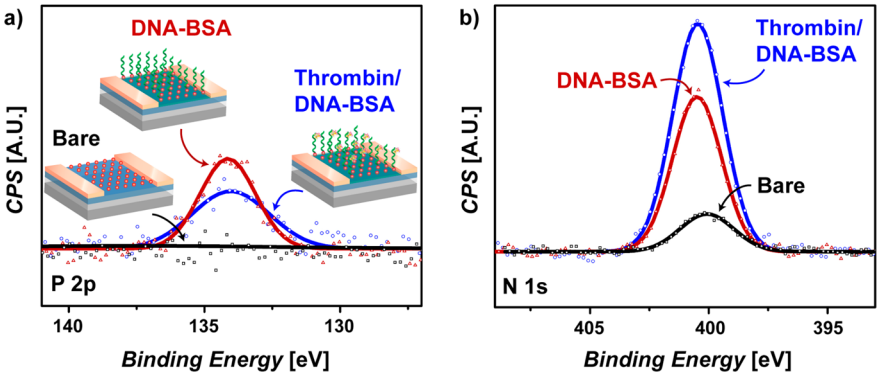

Figure 1. XPS characterization of sensor functionalization. (a) Phosphorus (P 2p) and (b) nitrogen (N 1s) XPS cross sections of the bare surface (black lines), the surface after functionalization with DNA and blocking with BSA (red lines), and the surface after exposure to thrombin (blue lines).

was confirmed with X-ray photoelectron spectroscopy (XPS) by monitoring the surface content of phosphorus (P 2p) and nitrogen (N 1s) (Figure 1). Prior to functionalization with DNA, there was no detectable phosphorus signal, and only residual nitrogen remained from the PS-P2VP matrix from which the AuNPs were cast (Figure 1, black lines). However, upon exposure of the AuNP-decorated platform to the thiolated DNA aptamer, a noticeable increase in the P 2p signal could be observed (Figure 1a, red line) as a result of the phosphate backbone of the DNA aptamer. Additionally, the presence of nitrogenous groups in both the DNA aptamer and BSA caused an increase in the magnitude of the N 1s peak as well as a +1 eV shift (Figure 1b, red line) as a result of their more electropositive chemical environments.[39,40] Exposure of the functionalized devices to thrombin attenuated the P 2p signal (Figure 1a, blue line), likely a result of the increased amount of protein on the surface rather than removal of DNA from the surface. This conclusion is supported by the further augmentation of the N 1s peak (Figure 1b, blue line), indicative of the presence of additional amino acid groups. XPS confirms successful functionalization of the device, which was completed in two simple incubation steps. Ease of functionalization of the AuNPs is a major advantage of this OFET platform, as is the large number of available thiolated receptor groups, allowing for a great variety of potential sensing targets using a single OFET platform.

Validation of Thrombin Sensitivity and Target Selectivity. Thrombin is a protease that is commonly used in model systems as a result of its thoroughly characterized interaction with a 15-mer DNA aptamer known to selectively bind thrombin with high specificity.[35−37] DNA aptamers have gained favor because of their cost effectiveness, stability to pH and temperature fluctuations, and insusceptibility to degradation.[41−45] Additionally, aptamers can be designed for a vast array of (bio)molecules, making this approach broadly applicable to a wide array of sensing targets. Here, aptamers are preferred over antibodies because the small size of the thrombin aptamer (~2 nm when folded)[44] compared to an antibody (~10−15 nm)[19] facilitates its use for charge-based detection in buffers of high ionic strength.[19] Additionally, the thrombin aptamer can be easily synthesized to contain a terminal thiol group, making it highly compatible with the AuNP-decorated OFET platform.

Prior to exposing the devices to thrombin, the system was allowed to fully equilibrate in a widely employed thrombin binding buffer (TBB, 1× TBB = 140 mM NaCl, 5 mM $MgCl_2$, 1 mM $CaCl_2$, 20 mM Tris-acetate, pH 5.5).[46] The device was operated at mild conditions (gate-source voltage (V_{GS}) = −0.4 V, drain-source voltage (V_{DS}) = −0.6 V) to prevent the electrolysis of the aqueous buffer (see Supporting Information, Figure S4 for source-drain current (I_{DS}) *vs* V_{GS} plots and Figure S5 for I_{DS} *vs* V_{DS} plots *in situ*). Delivery of thrombin to the OFET sensor was accomplished by means of a PDMS flow cell, mounted directly on top of the OFET and connected to an HPLC pump with polyether ether ketone (PEEK) tubing (Figure 2a), using a flow rate of 1 mL min^{-1}. The addition of thrombin to a device with AuNPs of d_{avg} ~ 70 nm operated in 0.0001× TBB, pH 5.5, resulted in a decrease in I_{DS} (Figure 2b). At this pH, thrombin has a net positive charge, as the pH is less than the isoelectric point (pI) of thrombin (7.0−7.6).[45,47] The increased positive charge density that develops on the surface of the OFET induces negative charges in the semiconductor according to the field effect,[48] which results in a decrease in the magnitude of I_{DS} in the p-type transistor. A similar trend in response has been observed before for the detection of small molecules,[49] DNA oligomers,[50] and ions[17,51] using FET-based sensors.

Under these operating conditions (0.0001× TBB, pH 5.5, d_{avg} ~ 70 nm), the detection limit for thrombin was 100 pM, well within the reported range of most other FET sensors[52−55] without the limitations typically associated with nanotube and nanowire-based FETs (tedious fabrication and low device-to-device reproducibility).[56] To allow for a more quantitative comparison, we plotted the sensitivity of our device *vs* thrombin concentration ($c_{thrombin}$) (Figure 2c), with the sensitivity of the device

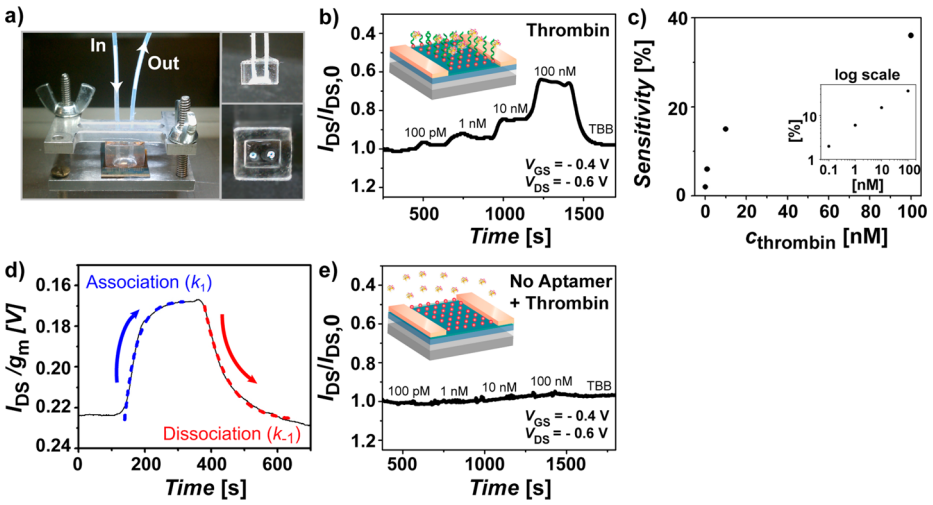

Figure 2. Validation of thrombin detection in 0.0001× TBB, pH 5.5 for a device decorated with AuNP of $d_{avg} \sim 70$ nm functionalized with thrombin binding aptamer. (a) PDMS flow cell used to deliver thrombin mounted directly on top of the OFET device. Insets show side and bottom view of the flow cell. (b) Response of the DNA-functionalized device to thrombin. (c) Plot of sensitivity *vs* analyte concentration ($c_{thrombin}$). Inset is log-scale plot. (d) Determination of the equilibrium dissociation constant (k_D) by fitting association and subsequent dissociation of thrombin/aptamer complex (dashed lines are exponential fits of curve). (e) Response of a device lacking the thrombin aptamer to thrombin.

being defined as

$$\text{sensitivity} = \frac{|I_{DS} - I_{DS,0}|}{I_{DS,0}} \quad (1)$$

We observed that sensitivity scales nonlinearly with increasing $c_{thrombin}$, which may be attributed an imperfect association between thrombin and its aptamer due to the low salt concentration as well as the potential of the protein to aggregate,[57] resulting in a multivalent binding event. Further, we estimated the equilibrium dissociation constant (k_D) of the thrombin aptamer−thrombin complex using the Langmuir binding isotherm. Various $c_{thrombin}$ were exposed to the sensor, followed by sensor regeneration with TBB (Figure 2d). I_{DS} was normalized by the transconductance (g_m) of the device (taken from the linear region of the conductance (I_{DS}/V_{DS}) *vs* V_{GS}) plot. Using the method presented by Duan *et al.*,[58] the association (k_1) and dissociation (k_{-1}) constants were determined from the normalized plot (see Supporting Information for more detailed discussion of this fit); k_D can be defined as

$$k_D = \frac{k_{-1}}{k_1} \quad (2)$$

Notably, k_D for the thrombin−aptamer complex was determined to be ∼140 nM, which is consistent with the value reported in literature for this aptamer.[35,37] Next, we analyzed the specificity of our platform. To ensure that the decrease in I_{DS} resulted from the binding of thrombin to its aptamer rather than through the nonspecific adsorption of thrombin onto the sensor surface, a device lacking the aptamer was exposed to thrombin. Figure 2e shows the lack of response of this unfunctionalized device to thrombin, indicating that no binding reaction occurs. This result suggests that a binding event must occur to induce a change in I_{DS}.

To further evaluate the platform's selectivity for thrombin, we interrogated it with other proteases (chymotrypsin and elastase), which mimic thrombin in size and pI (Figure 3a,b, respectively).[44,59,60] The device had only a minor response to both chymotrypsin (pI = 8.75) and elastase (pI = 8.5). The slight decrease in I_{DS} observed upon exposure to these proteins is likely caused by their overall high net positive charge (as discussed in the following sections) and not to a specific binding event,[55] as evidenced by the dramatically smaller magnitude of the change in I_{DS} for these proteins *vs* that observed for thrombin. Finally, the three serum proteases were combined and exposed to the sensor to evaluate potential interference caused by their interaction in solution (Figure 3c). The response is similar in magnitude to that of thrombin alone, suggesting that the presence of additional proteins does not affect the platform's ability to detect thrombin. Our experiments lead to the overall conclusion that the platform is sensitive to thrombin *via* the specific interaction with its DNA aptamer. The use of a flow cell coupled to a liquid delivery system to introduce analytes resulted in highly reproducible responses. Failure of other proteases to produce false positive results or interfere with the detection of thrombin indicates the platform's robustness.

Effect of Ionic Strength on Thrombin Detection. After thrombin detection had been successfully validated, we systematically analyzed the effect of varying the previously described parameters on biodetection. Our initial study was of the influence of charge screening on biodetection, a parameter that has attracted attention

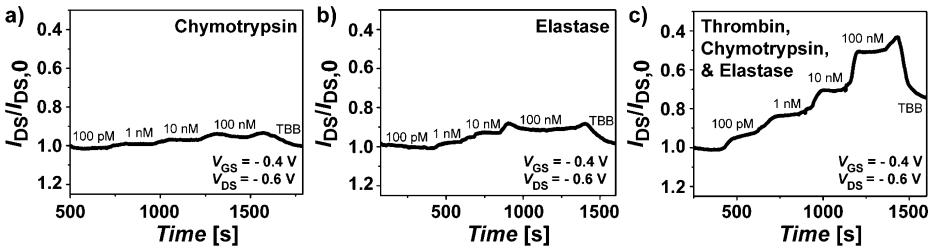

Figure 3. Demonstration of sensor selectivity. Response of the device to various proteases, including (a) chymotrypsin, (b) elastase, and (c) a combination of the three proteins.

for several decades.[61,62] For inorganic FETs, it has already been demonstrated that the ionic strength of the buffer has the single most influence on the sensitivity of the sensor[33] as a result of its inverse square root relationship with the charge screening distance (κ^{-1}), more commonly known as the Debye length; κ^{-1} is defined in as

$$\kappa^{-1} = \sqrt{\frac{\varepsilon k_B T}{2N_A e^2 I}} \quad (3)$$

where ε is the absolute permittivity of the electrolyte, k_B is Boltzmann's constant, T is the temperature, N_A is Avogadro's number, e is the charge of an electron, and I is the ionic strength of the solution, defined as

$$I = \frac{1}{2}\sum_{i=1}^{n} c_i z_i^2 \quad (4)$$

Here, c_i is the molar concentration of the ion, and z_i is the charge of the ion. As evidenced by Eq 3, κ^{-1} varies with the inverse square root of I; in 1× TBB, $\kappa^{-1} \sim 0.8$ nm, whereas $\kappa^{-1} \sim 8$ nm in 0.01× TBB, and $\kappa^{-1} \sim 80$ nm in 0.0001× TBB (Figure 4a). As many biological reactions are optimized at physiological ionic strengths (~100 mM), the screening occurring in 1× TBB (~140 mM) is most representative of that expected in complex biofluids.

To study this effect, we varied the concentration of the buffer (c_{TBB}) over a range between 0.0001× and 1× TBB while holding the other operating conditions (d_{avg} ~ 70 nm, pH 5.5) constant. The use of thrombin as a model system is again a good choice; the interaction between thrombin and its aptamer is highly robust and has been reported to occur readily, even at low ionic strengths.[45] We observed the largest response in a low ionic strength buffer (Figure 2b). The signal decreased by approximately a factor of 2 when c_{TBB} was increased to 0.01× (Figure 4b), and as a result, the detection limit increased to 1 nM. The sensitivity varied nonlinearly (but with a log−log relationship) with $c_{thrombin}$ at each c_{TBB} (Supporting Information, Figure S6a).

A further increase of c_{TBB} to 1× resulted in a vanishing signal change in I_{DS} (Figure 4c). At this buffer concentration, we observed a sharp decrease in I_{DS} and quick recovery to baseline following each switch in $c_{thrombin}$, which is attributed to the accompanying change in flow. We note that the response of OFETs to changes in flow has been observed previously[16] and does not affect thrombin detection. This inability to measure detection events in high ionic strength buffers is commonly perceived as a major limitation of FET-based sensors, as the optimal performance of many biomolecules and their biochemical reactions occur at ionic strengths mimicking physiological environments. In these conditions, ionic screening will limit the charge detection due to the formation of an electrostatic double layer.[18,20] For this reason, most of the experiments involving FETs are performed in buffer that has been greatly diluted or using systems that are insensitive to ionic strength.[18,20,61,64] Our results can be visualized in terms of the relationship between the sensitivity of the device and c_{TBB} (Figure 4d) in order to better understand these limitations. Our findings are in agreement with those in the literature for inorganic FETs but demonstrate that, despite vanishing signal in 1× TBB, several solutions exist to permit OFET-based detection at higher ionic strengths. First, a 10-fold reduction in buffer concentration or sample desalting (to 0.1× TBB) could be used to detect meaningful concentrations of thrombin at measurable sensitivities. Further, the biomolecules can be brought closer to the OFET interface by using aptamers in place of antibodies due to their smaller size in order to overcome screening limitations.[19] Currently, we are working toward developing closer interfaces in order to better understand the screening limitations of our platform.

Effect of AuNP Spacing on Thrombin Detection. The number of receptor groups present on the surface is likely to play a critical role in determining the dynamic range of the sensor. The number of aptameric receptor groups will be determined both by the total number of AuNPs present on the surface of the sensor in addition to the DNA loading per AuNP. A unique feature of our system is that d_{avg} can be easily tuned by varying the M_n of the PS-P2VP used to cast the AuNPs onto the surface. This method allows for facile control over the surface density of binding sites, as opposed to drop casting colloidal AuNPs onto the surface of the device, which was previously found to delaminate the electrodes.[17] Three d_{avg} values were investigated in this study, namely, ~40, ~70, and ~160 nm, which were cast from polymers of M_n of 34, 105, and 1376 kDa, respectively. D_{AuNP} was determined to be 4.8 ± 0.6, 10.3 ± 0.9, and 10.1 ± 3.6 nm for

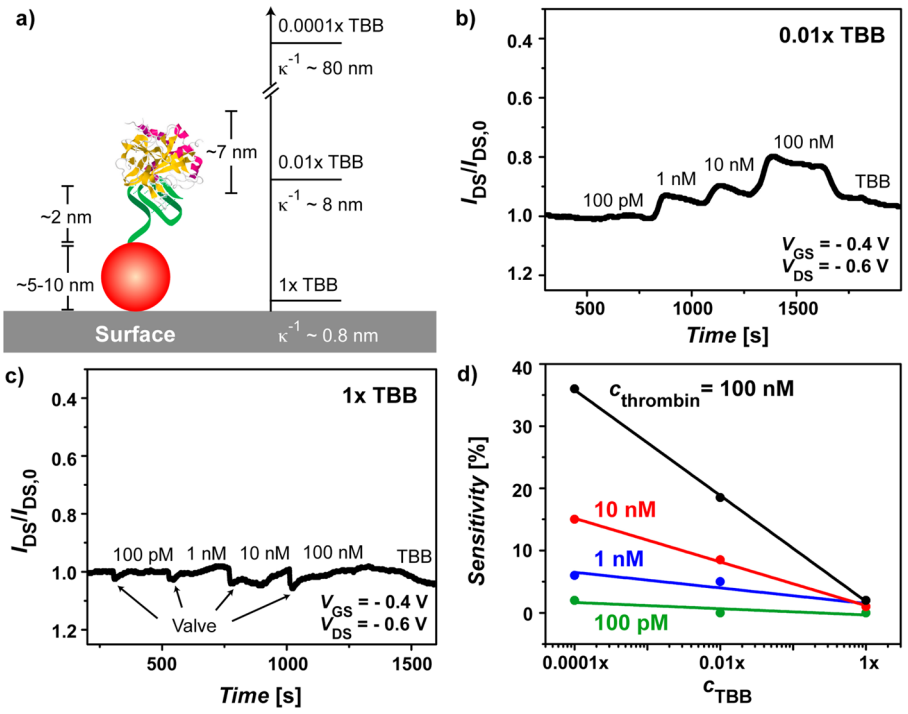

Figure 4. Effect of ionic strength variation on thrombin detection. (a) Relative size of the system components and visualization of the Debye screening length (κ^{-1}) at each buffer concentration (c_{TBB}). Drawing is not to scale and does not attempt to depict exact binding structure of the thrombin−aptamer complex. The average diameter of the AuNPs (D_{AuNP}) is ~5−10 nm, the DNA aptamer is ~2 nm in its folded configuration,[53] and thrombin can be roughly approximated as a sphere of diameter ~7 nm.[63] Thrombin detection response in (b) 0.01× and (c) 1× TBB. For thrombin response in 0.0001× TBB, see Figure 2b. Average AuNP spacing (d_{avg}) and pH were maintained at ~70 nm and 5.5, respectively. The abrupt changes in source-drain current (I_{DS}) occurring every ~250 s and quick recovery to baseline I_{DS} in (c) result from switching inlet ports and are an artifact of the corresponding change in flow[16] rather than detection events. (d) Device sensitivity *vs* c_{TBB} over the range of conditions tested (lines represent fit of data).

AuNPs cast from 34, 105, and 1376 kDa PS-P2VP, respectively. DNA loading per AuNP is dependent on the size of the AuNPs. The DNA loading was quantified through spectrophotometric measurement of the DNA released from the AuNPs after dissolution in 100 mM NaCN and was determined to be 2.9 ± 0.5 DNA/AuNP for the AuNPs cast from the 34 kDa PS-P2VP and 9.2 ± 1.8 DNA/AuNP for the AuNPs cast from the 105 kDa PS-P2VP. Quantification of the DNA loading on the AuNPs cast from the 1376 kDa PS-P2VP was not possible with this method due to the high level of salt contamination and the low quantity of DNA on the surface. However, since the DNA aptamer was introduced to the surface at a high molar excess, the same efficiency for the random deposition of DNA onto the AuNPs at each d_{avg} can be assumed.[65] Figure 5 summarizes our findings for this section.

Under the same operating conditions (0.0001× TBB, pH 5.5), we observed a greater signal for a given $c_{thrombin}$ using devices with d_{avg} ~ 40 nm (Figure 5a) when compared to devices with d_{avg} ~ 70 nm (Figure 5b) and d_{avg} ~ 160 nm (Figure 5c). At d_{avg} ~ 160 nm, the detection limit for thrombin was increased to 10 nM as a result of the lower number of binding sites available on the surface. Because both D_{AuNP} (which affects the DNA loading per AuNP) and d_{avg} (which affects the total number of AuNPs on the surface) were found to vary with different M_n PS-P2VP, the relationship between sensitivity and d_{avg} was not a simple inverse squared relationship, as would otherwise be expected. However, the sensitivity was found to vary according to a log−log relationship with $c_{thrombin}$ at each d_{avg} (Supporting Information, Figure S6b). These findings are in agreement with simulation studies which have indicated that increasing the receptor density on a FET can result in an increase in sensitivity.[34] This important result suggests that the dynamic range of these sensors can be tuned by varying the spacing between the AuNPs. At the low end, the detection limit can be decreased by spacing the AuNPs very closely together, with the spacing being limited only by the M_n of the polymers available to cast the AuNPs. Of the different M_n values investigated in this study, the 34 kDa PS-P2VP was the smallest block copolymer capable of forming stable micelles for the given deposition conditions. However, lower M_n versions of stable PS-P2VP could be synthesized to consist of a different M_n ratio between PS and P2VP blocks. At the high end, by using polymers of large M_n, the detection limit can be dramatically increased to allow for the detection of molecules whose relevant regime occurs at higher concentrations

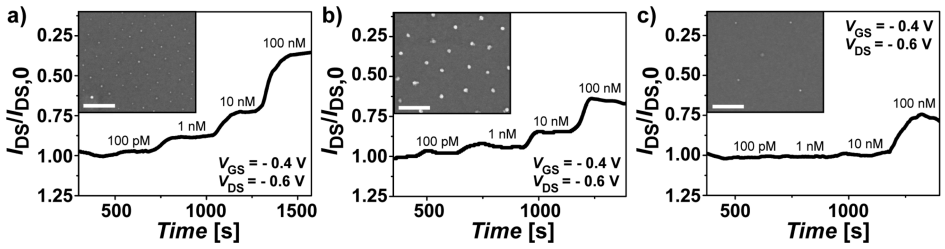

Figure 5. Effect of variation of AuNP spacing on thrombin detection. Sensing response to thrombin using devices with an average AuNP spacing (d_{avg}) of (a) ~40, (b) ~70, and (c) ~160 nm in 0.0001× TBB, pH 5.5. Insets are SEM images of AuNP-decorated surfaces. SEM scale bar = 100 nm.

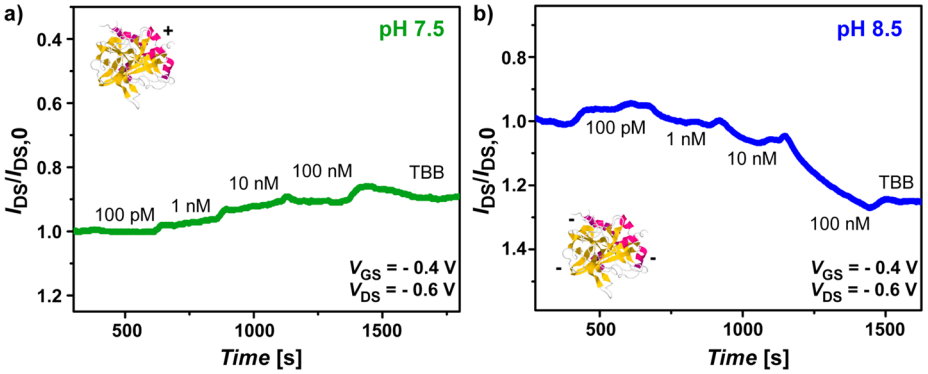

Figure 6. Effect of pH variation on thrombin detection. Thrombin detection using devices with an average AuNP spacing (d_{avg}) of ~70 nm in 0.0001× TBB at (a) pH 7.5 and (b) 8.5. Response of device to thrombin at pH 5.5 is shown in Figure 2b. Net charge of thrombin is approximately ~+8 at pH 5.5, ~+1 at pH 7.5, and ~−3 at pH 8.5.

(*e.g.*, blood glucose). We stress here that the use of block copolymer templating to produce ordered arrays of AuNPs provides a convenient mechanism by which the spacing of the receptor sites on the OFET's surface can be carefully controlled. Our finding does not only hold for our OFET system but also can be applied to general FET-based biodetection schemes; by tuning the density of the receptor sites in close vicinity to the channel, we could similarly manipulate the sensitivity.

Effect of pH on Thrombin Detection. The human body and its constituent biomolecules are highly sensitive to pH changes. Especially for proteins, an important consequence of pH variation is manipulation of the net charge of the molecule. In general, at a pH below its pI, a protein will have a positive net charge, while for a pH above its pI, it will have a negative net charge. The net charge of a protein can be approximated by calculating the number of charged residues present at a particular pH (Supporting Information, Figure S7 and Table S4).[33] In this study, the pH was varied between 5.5 and 8.5 while maintaining the other parameters (0.0001× TBB, d_{avg} ~ 70 nm) constant in order to understand the effect of the sign and magnitude of the analyte's charge on detection. Due to the nature of the binding between the DNA aptamer and thrombin, we do not expect that their interaction will significantly alter the pI of thrombin (7.0−7.6).[66,67] At pH 5.5, thrombin is highly positively charged in solution (Supporting Information, Table S4), and we observe a decrease in I_{DS} (Figure 2b). By increasing the pH to 7.5, which is near the pI of thrombin, the sensing response is greatly diminished (Figure 6a) as a result of the decrease in magnitude of net charge associated with the protein (Supporting Information, Table S4).

Next, we increased the pH to 8.5. At this pH, the net charge of thrombin is reversed, so that it becomes negatively charged in solution (Supporting Information, Table S4). Interestingly, by reversing the charge of the thrombin analyte from net positive to net negative, we observed an opposite response in our sensor. Specifically, upon introduction of thrombin to the device at pH 8.5, we observed an increase in I_{DS} (Figure 6b). This increase in I_{DS} is indicative of the accumulation of negative charge density near the surface of the OFET, which induces positive charges in the semiconductor according to the field effect.[17,49,51] Additionally, as the absolute value of the charge is less at pH 8.5 than at pH 5.5, the detection limit was increased to 1 nM. These trends are consistent with those previously observed in inorganic FET systems in which the sign of the analytes charge was varied,[10,23−26] as well as those predicted from simulation.[33] The sensitivity was found to scale nonlinearly with $c_{thrombin}$ at each pH (Supporting Information, Figure S6c); however, the two were found to vary with a log−log relationship. These experiments clearly demonstrate that the analyte must possess a sufficient net charge for successful detection with an OFET. While it has already been shown that a vanishing signal near the pI can be exploited to perform

rapid pI determination in proteins[10,23] and in biofunctionalization techniques,[68] no one has yet sought to intentionally increase detection sensitivity of an OFET by tuning a protein's charge by changing the pH. Our findings indicate that sensitivity of a FET biosensor, which is correlated with the net charge of the analyte, can be manipulated by varying the pH of the buffer solution. We stress that this process adds an important additional parameter in tuning the sensitivity of FET sensing systems.

CONCLUSION

In this report, we presented a detailed study of biodetection with OFETs, an important endeavor that has remained largely uninvestigated despite the promise of OFETs as diagnostic tools. Specifically, we demonstrated the selective detection of thrombin to 100 pM *in situ* using a AuNP-decorated OFET platform, and we performed a comprehensive examination to investigate the limiting factors governing biodetection with OFETs. To this end, we explored how the ionic strength and pH of the buffer as well as the density of the receptor sites affected the detection profile. Investigation of the effect of the buffer's ionic strength on detection revealed that, while charge screening prohibits charge-based OFET thrombin detection at high (>100 nM) ionic strengths, this limitation may be overcome by a 10-fold reduction in ionic strength to allow for measurable detection of the target protein. The use of DNA aptamers instead of antibodies decreased the size of the binding receptors, which also helped negate the effects of charge screening. By varying the M_n of the PS-P2VP from which the AuNPs were cast, we altered both the spacing and size of the AuNPs, permitting us to study the effect of receptor site spacing on the OFET's detection capability. Our investigation revealed that tuning the number of available receptor groups on the surface allows for control over the dynamic range of our sensor. This finding is important as it highlights the flexibility of a single sensor platform to be used for the detection of a variety of compounds with different relevant concentration ranges simply by tuning the number of receptor groups present. As a last step, we manipulated the analyte's charge by varying the pH of the buffer to better understand its effect on thrombin detection. We demonstrated that both the sign and magnitude of charge drastically affect the detection profile and detection limit of the sensor. In general, increasing the overall net charge of the protein analyte resulted in increased sensitivity, which could be controlled by adjusting the pH of the buffer. Overall, this work provides a comprehensive study of the factors affecting protein biodetection with OFETs. These findings provide a method by which the sensitivity of a biosensor can be tuned to better match that required for a particular biodetection application.

METHODS

Device Fabrication and AuNP Deposition. OFETs were fabricated as previously described,[12,17] with an ultrathin polymer dielectric layer and a water-stable organic semiconductor. These components permit the device's operation under water. DDFTTF, the semiconductor material, was synthesized and purified according to literature procedures.[17] The dielectric layer, a cross-linked polymer (PVP-HDA), was formed according to literature procedures[69] and spin-coated at 4500 rpm onto highly doped (n++), ⟨100⟩ orientation, native oxide Si wafers (Silicon Quest International). A 70 nm film of DDFTTF was deposited at a rate of 0.2 A s^{-1} on a heated substrate (195 °C) *via* thermal evaporation (Angstrom Engineering). $HAuCl_4$-containing PS-P2VP (34 kDa: M_n(PS) = 23.6 kDa, M_n(P2VP) = 10.4 kDa; 105 kDa: M_n(PS) = 55 kDa, M_n(P2VP) = 50 kDa; 1376 kDa: M_n(PS) = 1300 kDa, M_n(P2VP) = 76 kDa) solutions were prepared and deposited onto devices as previously reported.[17,70] The polymer matrix was subsequently removed by exposing the device to oxygen plasma (GaLa Instrumente) for 0.3 min (0.4 mbar of O_2, 80 W). Top contacts were deposited *via* the thermal evaporation of Au (channel width = 4 mm, channel length = 50 μm) through a shadow mask on a rotating substrate at a rate of 0.4 A s^{-1}. A 50 nm film of SiO_x was thermally evaporated exclusively onto electrodes at a rate of 0.4 A s^{-1} to passivate them from potential electrochemical reactions and DNA functionalization.

AuNP Functionalization. Pre-existing AuNP arrays were cleaned with a 0.1 min re-exposure to oxygen plasma. A thiolated 15-mer DNA oligonucleotide sequence that was previously reported to bind thrombin (5′-$(CH_2)_6$-S-S-$(CH_2)_6$-TAA GTT CAT CTC CCC **GGT TGG TGT GGT TGG** T-3′)[35,36] was custom synthesized by Integrated DNA Technologies. Basepairs shown in bold indicate those responsible for imparting selectivity for thrombin. The aptamer was heated to 95 °C for 3 min and slowly cooled to room temperature to obtain the proper conformation.[45,71] 8 μL of a 100 μM DNA solution in 0.0001x TBB, pH 5.5 was then spotted onto the devices, followed by incubation at room temperature for 60 min in a desiccator under slight vacuum. The optimal conditions for the BSA blocking step were determined to be incubation in a 0.1% solution of BSA in 1× phosphate buffered saline (PBS, 1× PBS = 137 mM NaCl, 2.7 mM KCl, 10 mM Na_2HPO_4, 2 mM KH_2PO_4, pH 7.4) for 60 min (Supporting Information, Figure S3). Following DNA incubation and BSA blocking, the devices were rinsed in deionized water and placed under vacuum to dry.

Device Characterization. The elemental composition of the surfaces was measured with XPS (PHI 5000 Versaprobe, Al Kα source). High-resolution spectra were collected at a pass energy of 117.4 eV, an angle of 45°, and a step size of 0.1 eV. All XPS spectra were referenced to a C 1s binding energy of 284.8 eV. The surfaces on which XPS measurements were performed contained an additional layer of spin-coated AuNPs to increase the AuNP density.[17,70] Interparticle spacing was characterized using a MultiMode AFM (Veeco) operated in the tapping mode, while D_{AuNP} was characterized using an XHR SEM (FEI Magellan).[72] DNA loading was quantified through spectrophotometric measurement (NanoDrop 1000) of the DNA released from the AuNPs after treatment with a 100 mM NaCN solution.[73,74] Electrical measurements were carried out under ambient conditions using sourcemeters (Keithley 2635 for drain/source voltage and Keithley 2400 for gate voltage).

Flow Cell Setup and Liquid Delivery. For electrical testing under aqueous conditions, a PDMS flow cell with an internal volume of 66 μL was mounted on top of the device. PEEK tubing with 0.0625 in. internal diameter connected the flow cell to an HPLC pump (Lab Alliance Series III). TBB solutions were freshly prepared immediately prior to measurement at concentrations of 0.0001, 0.01, and 1×. The pH of each solution was adjusted using

10 mM KOH to pH ~5.5, ~7.5, or ~8.5, as verified with pH paper and a pH meter. These solutions were delivered to the pump *via* a 10-port valve (VICI Cheminert Line). Prior to *in situ* testing, each device was allowed to thoroughly equilibrate to aqueous conditions for 1 h. A low operating voltage ($V_{DS} = -0.6$ V, $V_{GS} = -0.4$ V) was used in order to prevent ionic conduction through the liquid (Supporting Information, Figures S4 and S5). Human α-thrombin was purchased in a 50% glycerol/water solution (Haematologic Technologies, Inc.). Solutions of α-thrombin, elastase (Promega Co.), and α-chymotrypsin (MP Biomedicals) were generated through serial dilution in freshly made TBB buffer to final concentrations of 100 pM, 1 nM, 10 nM, and 100 nM. The pH of each solution was subsequently adjusted using 10 mM KOH to pH ~5.5, ~7.5, or ~8.5, as verified with both pH paper and a pH meter. Two milliliters each of these testing solutions was delivered to the OFET at a flow rate of 1.0 mL min^{-1}. Between additions, the flow rate was reduced to 0.1 mL min^{-1} and the response was allowed to equilibrate.

Conflict of Interest: The authors declare no competing financial interest.

Acknowledgment. The authors thank O. B. Johnson for many helpful discussions, M. Vosgueritchian for assistance with SEM measurements, and D. W. Lin for assistance with DNA quantification. M.L.H. acknowledges funding from the National Defense Science and Engineering Graduate (NDSEG) Fellowship (32 CFR 168a) and the National Science Foundation Graduate Research Fellowship. O. K. acknowledges financial support from the Swiss National Science Foundation (PBBSP2-138715). Both a Gates Foundation Grand Challenges Explorations Grant (OPP1032970) and a National Science Foundation Grant (NSF ECCS 1101901) also funded this work.

Supporting Information Available: More extensive characterization of AuNP spacing and DNA loading, device functionalization and operation, as well as a discussion of methodology to obtain binding parameters and calculate protein net charge. This material is available free of charge *via* the Internet at http://pubs.acs.org.

REFERENCES AND NOTES

1. Yager, P.; Domingo, G. J.; Gerdes, J. Point-of-Care Diagnostics for Global Health. *Annu. Rev. Biomed. Eng.* **2008**, *10*, 107–144.
2. Roberts, M. E.; Sokolov, A. N.; Bao, Z. Material and Device Considerations for Organic Thin-Film Transistor Sensors. *J. Mater. Chem.* **2009**, *19*, 3351–3363.
3. Knopfmacher, O.; Tarasov, A.; Wipf, M.; Fu, W.; Calame, M.; Schönenberger, C. Silicon-Based Ion-Sensitive Field-Effect Transistor Shows Negligible Dependence on Salt Concentration at Constant pH. *ChemPhysChem* **2012**, *13*, 1157–1160.
4. Sokolov, A. N.; Roberts, M. E.; Bao, Z. Fabrication of Low-Cost Electronic Biosensors. *Mater. Today* **2009**, *12*, 12–20.
5. Casalini, S.; Leonardi, F.; Cramer, T.; Biscarini, F. Organic Field-Effect Transistor for Label-Free Dopamine Sensing. *Org. Electron.* **2013**, *14*, 156–163.
6. Owens, R. M.; Malliaras, G. G. Organic Electronics at the Interface with Biology. *MRS Bull.* **2010**, *35*, 449–456.
7. Torsi, L.; Dodabalapur, A.; Sabbatini, L.; Zambonin, P. G. Multi-parameter Gas Sensors Based on Organic Thin-Film-Transistors. *Sens. Actuators, B* **2000**, *67*, 312–316.
8. Torsi, L.; Dodabalapur, A.; Cioffi, N.; Sabbatini, L.; Zambonin, P. G. NTCDA Organic Thin-Film Transistor as Humidity Sensor: Weaknesses and Strengths. *Sens. Actuators, B* **2001**, *77*, 7–11.
9. Mabeck, J. T.; Malliaras, G. G. Chemical and Biological Sensors Based on Organic Thin-Film Transistors. *Anal. Bioanal. Chem.* **2006**, *384*, 343–353.
10. Khan, H. U.; Jang, J.; Kim, J.-J.; Knoll, W. *In Situ* Antibody Detection and Charge Discrimination Using Aqueous Stable Pentacene Transistor Biosensors. *J. Am. Chem. Soc.* **2011**, *133*, 2170–2176.
11. Khan, H. U.; Roberts, M. E.; Johnson, O.; Förch, R.; Knoll, W.; Bao, Z. *In Situ*, Label-Free DNA Detection Using Organic Transistor Sensors. *Adv. Mater.* **2010**, *22*, 4452–4456.
12. Roberts, M. E.; Mannsfeld, S. C. B.; Queralto, N.; Reese, C.; Locklin, J.; Knoll, W.; Bao, Z. Water-Stable Organic Transistors and Their Application in Chemical and Biological Sensors. *Proc. Natl. Acad. Sci. U.S.A.* **2008**, *105*, 12134–12139.
13. Angione, M. D.; Cotrone, S.; Magliulo, M.; Mallardi, A.; Altamura, D.; Giannini, C.; Cioffi, N.; Sabbatini, L.; Fratini, E.; Baglioni, P.; *et al.* Interfacial Electronic Effects in Functional Biolayers Integrated into Organic Field-Effect Transistors. *Proc. Natl. Acad. Sci. U.S.A.* **2012**, *109*, 6429–6434.
14. Tisch, U.; Haick, H. Nanomaterials for Cross-Reactive Sensor Arrays. *MRS Bull.* **2010**, *35*, 797–803.
15. Bazan, G. C.; Wang, S. Organic Semiconductors in Sensor Applications. In *Springer Series in Materials Science*; Bernards, D. A., Owens, R. M., Malliaras, G. G., Eds.; Springer: New York, 2008; pp 1–23.
16. Someya, T.; Dodabalapur, A.; Gelperin, A.; Katz, H. E.; Bao, Z. Integration and Response of Organic Electronics with Aqueous Microfluidics. *Langmuir* **2002**, *18*, 5299–5302.
17. Hammock, M. L.; Sokolov, A. N.; Stoltenberg, R. M.; Naab, B. D.; Bao, Z. Organic Transistors with Ordered Nanoparticle Arrays as a Tailorable Platform for Selective, *In Situ* Detection. *ACS Nano* **2012**, *6*, 3100–3108.
18. Kulkarni, G. S.; Zhong, Z. Detection beyond the Debye Screening Length in a High-Frequency Nanoelectronic Biosensor. *Nano Lett.* **2012**, *12*, 719–723.
19. Maehashi, K.; Katsura, T.; Kerman, K.; Takamura, Y.; Matsumoto, K.; Tamiya, E. Label-Free Protein Biosensor Based on Aptamer-Modified Carbon Nanotube Field-Effect Transistors. *Anal. Chem.* **2007**, *79*, 782–787.
20. Stern, E.; Wagner, R.; Sigworth, F. J.; Breaker, R.; Fahmy, T. M.; Reed, M. A. Importance of the Debye Screening Length on Nanowire Field Effect Transistor Sensors. *Nano Lett.* **2007**, *7*, 3405–3409.
21. Zhang, G.-J.; Zhang, G.; Chua, J. H.; Chee, R.-E.; Wong, E. H.; Agarwal, A.; Buddharaju, K. D.; Singh, N.; Gao, Z.; Balasubramanian, N. DNA Sensing by Silicon Nanowire: Charge Layer Distance Dependence. *Nano Lett.* **2008**, *8*, 1066–1070.
22. Gao, A.; Lu, N.; Wang, Y.; Dai, P.; Li, T.; Gao, X.; Want, Y.; Fan, C. Enhanced Sensing of Nucleic Acids with Silicon Nanowire Field Effect Transistor Biosensors. *Nano Lett.* **2012**, *12*, 5262–5268.
23. Patolsky, F.; Zheng, G.; Hayden, O.; Lakadamyali, M.; Zhuang, X.; Lieber, C. M. Electrical Detection of Single Viruses. *Proc. Natl. Acad. Sci. U.S.A.* **2004**, *101*, 14017–14022.
24. Stern, E.; Klemic, J. F.; Routenberg, D. A.; Wyrembak, P. N.; Turner-Evans, D. B.; Hamilton, A. D.; LaVan, D. A.; Fahmy, T. M.; Reed, M. A. Label-Free Immunodetection with CMOS-Compatible Semiconducting Nanowires. *Nature* **2007**, *445*, 519–522.
25. Cheng, Y.; Chen, K. S.; Meyer, N. L.; Yuan, J.; Hirst, L. S.; Chase, P. B.; Xiong, P. Functionalized SnO_2 Nanobelt Field-Effect Transistor Sensors for Label-Free Detection of Cardiac Troponin. *Biosens. Bioelectron.* **2011**, *26*, 4538–4544.
26. Ohno, Y.; Maehashi, K.; Matsumoto, K. Chemical and Biological Sensing Applications Based on Graphene Field-Effect Transistors. *Biosens. Bioelectron.* **2010**, *26*, 1727–1730.
27. Mabeck, J. T.; DeFranco, J. A.; Bernards, D. A.; Malliaras, G. G.; Hocdé, S. Microfluidic Gating of an Organic Electrochemical Transistor. *Appl. Phys. Lett.* **2005**, *87*, 013503.
28. Spijkman, M.-J.; Brondijk, J. J.; Geuns, T. C. T.; Smits, E. C. P.; Cramer, T.; Zerbetto, F.; Stoliar, P.; Biscarini, F.; Blom, P. W. M.; de Leeuw, D. M. Dual-Gate Organic Field-Effect Transistors as Potentiometric Sensors in Aqueous Solution. *Adv. Funct. Mater.* **2010**, *20*, 898–905.
29. Kergoat, L.; Piro, B.; Berggren, M.; Pham, M.-C.; Yassar, A.; Horowitz, G. DNA Detection with a Water-Gated Organic Field-Effect Transistor. *Org. Electron.* **2012**, *13*, 1–6.
30. Kergoat, L.; Piro, B.; Breggren, M.; Horowitz, G.; Pham, M.-C. Advances in Organic Transistor-Based Biosensors: From Organic Electrochemical Transistors to Electrolyte-Gated Organic Field Effect Transistors. *Anal. Bioanal. Chem.* **2012**, *402*, 1813–1826.

31. Haeberle, T.; Münzer, A. M.; Buth, F.; Garrido, J. A.; Abdellah, A.; Fabel, B.; Lugli, P.; Scarpa, G. Solution Processable Carbon Nanotube Network Thin-Film Transistors Operated in Electrolytic Solutions at Various pH. *Appl. Phys. Lett.* **2012**, *101*, 223101.
32. Cramer, T.; Kyndiah, A.; Murgia, M.; Leonardi, F.; Casalini, S.; Biscarini, F. Double Layer Capacitance Measured by Organic Field Effect Transistor Operated in Water. *Appl. Phys. Lett.* **2012**, *100*, 143302.
33. De Vico, L.; Sorensen, M. H.; Iversen, L.; Rogers, D. M.; Sorensen, B. S.; Brandbyge, M.; Nygard, J.; Martinez, K. L.; Jensen, J. H. Quantifying Signal Changes in Nano-wire Based Biosensors. *Nanoscale* **2011**, *3*, 706–717.
34. Islam, M. S.; Kouzani, A. Z. Design of a High Sensitive Double-Gate Field-Effect Transistor Biosensor for DNA Detection. *33rd Annual International Conference of IEEE Engineering Medicine and Biology Society*; Boston, MA, **2011**; pp 4788−4791.
35. Bock, L. C.; Griffin, L. C.; Latham, J. A.; Vermaas, E. H.; Toole, J. J. Selection of Single-Stranded-DNA Molecules That Bind and Inhibit Human Thrombin. *Nature* **1992**, *355*, 564–566.
36. Vairamani, M.; Gross, M. L. G-Quadruplex Formation of Thrombin-Binding Aptamer Detected by Electrospray Ionization Mass Spectrometry. *J. Am. Chem. Soc.* **2003**, *125*, 42–43.
37. Macaya, R. F.; Waldron, J. A.; Beutel, B. A.; Gao, H. T.; Joesten, M. E.; Yang, M. H.; Patel, R.; Bertelsen, A. H.; Cook, A. F. Structural and Functional-Characterization of Potent Antithrombotic Oligonucleotides Possessing Both Quadruplex and Duplex Motifs. *Biochemistry* **1995**, *34*, 4478–4492.
38. Sweryda-Krawiec, B.; Devaraj, H.; Jacob, G.; Hickman, J. J. A New Interpretation of Serum Albumin Surface Passivation. *Langmuir* **2004**, *20*, 2054–2056.
39. Lee, C. Y.; Gong, P.; Harbers, G. M.; Grainger, D. W.; Castner, D. G.; Gamble, L. J. Surface Coverage and Structure of Mixed DNA/Alkylthiol Monolayers on Gold: Characterization by XPS, NEXAFS, and Fluorescence Intensity Measurements. *Anal. Chem.* **2006**, *78*, 3316–3325.
40. Zhou, X.; Goh, S. H.; Lee, S. Y.; Tan, K. L. X-ray Photoelectron Spectroscopic Studies of Interactions between Poly(*p*-vinylphenol) and Poly(vinylpyridine)s. *Appl. Surf. Sci.* **1997**, *119*, 60–66.
41. Strehlitz, B.; Nikolaus, N.; Stoltenburg, R. Protein Detection with Aptamer Biosensors. *Sensors* **2008**, *8*, 4296–4307.
42. Torres-Chavolla, E.; Alocilja, E. C. Aptasensors for Detection of Microbial and Viral Pathogens. *Biosens. Bioelectron.* **2009**, *24*, 3175–3182.
43. Xu, Y.; Cheng, G.; He, P.; Fang, Y. A Review: Electrochemical Aptasensors with Various Detection Strategies. *Electroanalysis* **2009**, *21*, 1251–1259.
44. Lee, J.-O.; So, H.-M.; Jeon, E.-K.; Chang, H.; Won, K.; Kim, Y. H. Aptamers as Molecular Recognition Elements for Electrical Nanobiosensors. *Anal. Bioanal. Chem.* **2008**, *390*, 1023–1032.
45. Hianik, T.; Ostatná, V.; Sonlajtnerova, M.; Grman, I. Influence of Ionic Strength, pH and Aptamer Configuration for Binding Affinity to Thrombin. *Bioelectrochemistry* **2007**, *70*, 127–133.
46. Cho, H.; Baker, B. R.; Wachsmann-Hogiu, S.; Pagba, C. V.; Laurence, T. A.; Lane, S. M.; Lee, L. P.; Tok, J. B.-H. Aptamer-Based SERRS Sensor for Thrombin Detection. *Nano Lett.* **2008**, *8*, 4386–4390.
47. Fenton, J. W.; Fasco, M. J.; Stackrow, A. B.; Aronson, D. L.; Young, A. M.; Finlayson, J. S. Human Thrombins—Production, Evaluation, and Properties of α-Thrombin. *J. Biol. Chem.* **1977**, *252*, 3587–3598.
48. Park, Y. M.; Salleo, A. Dual-Gate Organic Thin Film Transistors as Chemical Sensors. *Appl. Phys. Lett.* **2009**, *95*, 133307.
49. Khan, H. U.; Roberts, M. E.; Knoll, W.; Bao, Z. Pentacene Based Organic Thin Film Transistors as the Transducer for Biochemical Sensing in Aqueous Media. *Chem. Mater.* **2011**, *23*, 1946–1953.
50. Stoliar, P.; Bystrenova, E.; Quiroga, S. D.; Annibale, P.; Facchini, M.; Spijkman, M.; Setayesh, S.; de Leeuw, D.; Biscarini, F. DNA Adsorption Measured with Ultra-thin Film Organic Field Effect Transistors. *Biosens. Bioelectron.* **2009**, *24*, 2935.
51. Maddalena, F.; Kuiper, M. J.; Poolman, B.; Brouwer, F.; Hummelen, J. C.; de Leeuw, D. M.; De Boer, B.; Blom, P. W. M. Organic Field-Effect Transistor-Based Biosensors Functionalized with Protein Receptors. *J. Appl. Phys.* **2010**, *108*, 124501.
52. Xie, H.; Luo, S.-C.; Yu, H.-H. Electric-Field-Assisted Growth of Functionalized Poly(3,4-ethylenedioxythiophene) Nanowires for Label-Free Protein Detection. *Small* **2009**, *5*, 2611–2617.
53. Kim, K. S.; Lee, H.-S.; Yang, J.-A.; Jo, M.-H.; Hahn, S. K. The Fabrication, Characterization and Application of Aptamer-Functionalized Si-Nanowire FET Biosensors. *Nanotechnology* **2009**, *20*, 235501.
54. Croce, R. A., Jr.; Vaddiraju, S.; Chan, P.-Y.; Seyta, R.; Jain, F. C. Label-Free Protein Detection Based on Vertically Aligned Carbon Nanotube Gated Field-Effect Transistors. *Sens. Actuators, B* **2011**, *160*, 154–160.
55. Düzgün, A.; Maroto, A.; Mairal, T.; O'Sullivan, C.; Rius, F. X. Solid-Contact Potentiometric Aptasensor Based on Aptamer Functionalized Carbon Nanotubes for the Direct Determination of Proteins. *Analyst* **2010**, *135*, 1037–1041.
56. Roberts, M. E.; LeMieux, M. C.; Bao, Z. Sorted and Aligned Single-Walled Carbon Nanotube Networks for Transistor-Based Aqueous Chemical Sensors. *ACS Nano* **2009**, *3*, 3287–3293.
57. D'Arcy, A. Crystallizing Proteins—A Rational Approach? *Acta Crystallogr.* **1994**, *50*, 469–471.
58. Duan, X.; Li, Y.; Rajan, N. K.; Routenberg, D. A.; Modis, Y.; Reed, M. A. Quantification of the Affinities and Kinetics of Protein Interactions Using Silicon Nanowire Biosensors. *Nat. Nanotechnol.* **2012**, *7*, 401–407.
59. Chen, C.-K.; Huang, C.-C.; Chang, H.-T. Label-Free Colorimetric Detection of Picomolar Thrombin in Blood Plasma Using a Gold Nanoparticle-Based Assay. *Biosens. Bioelectron.* **2010**, *25*, 1922–1927.
60. So, H.-M.; Won, K.; Kim, Y. H.; Kim, B.-K.; Ryu, B. H.; Na, P. S.; Kim, H.; Lee, J.-O. Single-Walled Carbon Nanotube Biosensors Using Aptamers as Molecular Recognition Elements. *J. Am. Chem. Soc.* **2005**, *127*, 11906–11907.
61. Poghossian, A.; Cherstvy, A.; Ingebrandt, S.; Offenhausser, A.; Schoning, M. J. Possibilities and Limitations of Label-Free Detection of DNA Hybridization with Field-Effect-Based Devices. *Sens. Actuators, B* **2005**, *111*, 470–480.
62. Schasfoort, R. B. M.; Bergveld, P.; Kooyman, R. P. H.; Greve, J. Possibilities and Limitations of Direct Detection of Protein Charges by Means of an Immunological Field-Effect Transistor. *Anal. Chim. Acta* **1990**, *238*, 323–329.
63. Skrzypczak-Jankun, E.; Rydel, T. J.; Tulinsky, A.; Fenton, J. W.; Mann, K. G. Human D-Phe-Pro-Arg-CH_2-α-Thrombin Crystallization and Diffraction Data. *J. Mol. Biol.* **1989**, *206*, 755–757.
64. Star, A.; Gabriel, J. C. P.; Bradley, K.; Gruner, G. Electronic Detection of Specific Protein Binding Using Nanotube FET Devices. *Nano Lett.* **2003**, *3*, 459–463.
65. Stoltenberg, R. M. A Self Assembly Approach to Localization and Patterning of Optically Resolved Single Molecules. Ph.D. Thesis, Stanford University 2011.
66. Padmanabhan, K.; Padmanabhan, K. P.; Ferrara, J. D.; Sadler, J. E.; Tulinsky, A. The Structure of α-Thrombin Inhibited by a 15-Mer Single-Stranded DNA Aptamer. *J. Biol. Chem.* **1993**, *268*, 17651–17654.
67. Paborsky, L. R.; McCurdy, S. N.; Griffin, L. C.; Toole, J. J.; Leung, L. K. The Single-Stranded DNA Aptamer-Binding Site of Human Thrombin. *J. Biol. Chem.* **1993**, *268*, 20808–20811.
68. Wijaya, E.; Lenaerts, C.; Maricot, S.; Hastanin, J.; Habraken, S.; Vilcot, J.-P.; Boukherroub, R.; Szunerits, S. Surface Plasmon Resonance-Based Biosensors: From the Development of Different SPR Structures to Novel Surface Functionalization Strategies. *Curr. Opin. Solid State Mater. Sci.* **2011**, *15*, 208–224.

69. Sokolov, A. N.; Cao, Y.; Johnson, O.; Bao, Z. Mechanistic Considerations of Bending-Strain Effects within Organic Semiconductors on Polymer Dielectrics. *Adv. Funct. Mater.* **2011**, *22*, 175.
70. Stoltenberg, R. M.; Liu, C.; Bao, Z. Selective Surface Chemistry Using Alumina Nanoparticles Generated from Block Copolymers. *Langmuir* **2011**, *27*, 445–451.
71. Bini, A.; Minunni, M.; Tombelli, S.; Centi, S.; Mascini, M. Analytical Performances of Aptamer-Based Sensing for Thrombin Detection. *Anal. Chem.* **2007**, *79*, 3016–3019.
72. Junno, T.; Deppert, K.; Montelius, L.; Samuelson, L. Controlled Manipulation of Nanoparticles with an Atomic Force Microscope. *Appl. Phys. Lett.* **1995**, *66*, 3627–3629.
73. Demers, L. M.; Mirkin, C. A.; Mucic, R. C.; Reynolds, R. A.; Letsinger, R. L.; Elghanian, R.; Viswanadham, G. A Fluorescence-Based Method for Determining the Surface Coverage and Hybridization Efficiency of Thiol-Capped Oligonucleotides Bound to Gold Thin Films and Nanoparticles. *Anal. Chem.* **2000**, *72*, 5535–5541.
74. Hurst, S. J.; Lytton-Jean, A. K. R.; Mirkin, C. A. Maximizing DNA Loading on a Range of Gold Nanoparticle Sizes. *Anal. Chem.* **2006**, *78*, 8313–8318.